LAWRENCE
LIVERMORE
NATIONAL
LABORATORY

LLNL-JRNL-769893

Uncertainty Propagation Analysis of Computational Models in Laser Powder Bed Fusion Additive Manufacturing Using Polynomial Chaos Expansions

G. Tapia, W. E. King, L. Johnson, R. Arroyave, I. Karaman, A. Elwany

March 18, 2019

Uncertainty Propagation Analysis of Computational Models in Laser Powder Bed Fusion Additive Manufacturing Using Polynomial Chaos Expansions

Disclaimer

This document was prepared as an account of work sponsored by an agency of the United States government. Neither the United States government nor Lawrence Livermore National Security, LLC, nor any of their employees makes any warranty, expressed or implied, or assumes any legal liability or responsibility for the accuracy, completeness, or usefulness of any information, apparatus, product, or process disclosed, or represents that its use would not infringe privately owned rights. Reference herein to any specific commercial product, process, or service by trade name, trademark, manufacturer, or otherwise does not necessarily constitute or imply its endorsement, recommendation, or favoring by the United States government or Lawrence Livermore National Security, LLC. The views and opinions of authors expressed herein do not necessarily state or reflect those of the United States government or Lawrence Livermore National Security, LLC, and shall not be used for advertising or product endorsement purposes.

Journal of Manufacturing Science and Engineering. Received November 08, 2017;
Accepted manuscript posted August 17, 2018. doi:10.1115/1.4041179
Copyright (c) 2018 by ASME

Uncertainty Propagation Analysis of Computational Models in Laser Powder Bed Fusion Additive Manufacturing using Polynomial Chaos Expansions

Gustavo Tapia
Industrial and Systems Engineering Department
Texas A&M University
College Station, TX 77843
Email: gtapia@tamu.edu

Wayne King
Physical and Life Sciences Directorate
Lawrence Livermore National Laboratory
Livermore, CA 94550
Email: weking@llnl.gov

Luke Johnson, Raymundo Arroyave, Ibrahim Karaman
Materials Science and Engineering Department
Texas A&M University
College Station, TX 77843

Alaa Elwany*
Industrial and Systems Engineering Department
Texas A&M University
College Station, TX 77843
Email: elwany@tamu.edu

Accepted Manuscript Not Copyedited

ABSTRACT

Computational models for simulating physical phenomena during laser-based powder bed fusion additive manufacturing (L-PBF AM) processes are essential for enhancing our understanding of these processes, enable process optimization, and accelerate qualification and certification of AM materials and parts. It is a well-known fact that such models typically involve multiple sources of uncertainty that originate from different sources such as model parameters uncertainty, or model/code inadequacy, among many others. Uncertainty quantification is a broad field that focuses on characterizing such uncertainties in order to maximize the benefit of these models. Although uncertainty quantification has been a center theme in computational models associated with diverse fields such as computational fluid dynamics and macro-economics, it has not yet been fully exploited with computational models for advanced manufacturing.

The current study presents one among the first efforts to conduct uncertainty propagation analysis in the context of L-PBF AM. More specifically, we present a generalized Polynomial Chaos Expansions framework to assess the distributions of melt pool dimensions due to uncertainty in input model parameters. We develop the methodology and then employ it to validate model predictions, both through benchmarking them against Monte Carlo methods and against experimental data acquired from an experimental testbed.

*Corresponding author.

Downloaded From: http://biomechanical.asmedigitalcollection.asme.org/ on 09/04/2018 Terms of Use: http://www.asme.org/about-asme/terms-of-use

Journal of Manufacturing Science and Engineering. Received November 08, 2017;
Accepted manuscript posted August 17, 2018. doi:10.1115/1.4041179
Copyright (c) 2018 by ASME

1 Introduction

Additive Manufacturing (AM) technologies have recently witnessed considerable advancement due to the research focus they have received over the past decade. This advancement has been very useful in identifying and prioritizing research needs necessary to further advance AM and unlock the opportunities and capabilities that it offers. Furthermore, new trends within the field have started to emerge including new alloy design, functional grading, and linking AM to cyberphysical systems in order to contribute to the fourth industrial revolution. In industrial sectors such as aerospace, automotive, and healthcare, many proven applications for metal-based AM technologies (and in particular, Laser-Based Powder Bed Fusion (L-PBF) processes) have been demonstrated. The capabilities of metal AM including geometric freedom, flexibility, part consolidation [1], design optimization and material waste reduction [2] are generally accepted by now.

In L-PBF processes, metallic parts are created from raw material in powder form. The material is laid down on a base substrate in the form of thin layers (usually less than 50μm), and then selectively fused with a high-power laser beam to melt and bond the powder particles in a layer by layer fashion, guided by a digital CAD model. Although the operating principle of L-PBF is relatively straightforward, the underlying physics of the process are far away from being simple and involve successive and very rapid melting, solidification, and re-melting of the processed material. This results in very complex thermal histories during processing, which makes the fabricated parts highly prone to manufacturing defects. Examples of these defects include porosity, gas entrapment, cracks, and lack of fusion. These defects can drastically alter part quality and performance. Consequently, the use of L-PBF parts in applications with stringent quality requirements such as aerospace components and biomedical devices requires for further study and improvement.

A myriad of L-PBF research studies have focused on defining process signatures and metrics that can serve as proxies for part quality. These signatures are extremely useful for conducting process monitoring and control [3]. Perhaps one of the most common signatures investigated in the literature is the *melt pool* [4–6], which refers to the region at the laser-powder interface where powder particles melt to form a pool of molten metal. Melt pool characteristics (geometry and temperature) are important since they provide an indication of how well adjacent tracks and successive layers bond to one another [7]. These characteristics largely depend on the proper selection of manufacturing processing parameters. Prior studies have indicated that up to 157 parameters can influence the L-PBF process in general [8, 9], but it is common to focus on laser parameters when considering melt pool characteristics. These primarily include laser power (P), laser scanning speed (v), and laser beam diameter ($D4$). Consequently, there is a need to study the influence of laser parameters on melt pool characteristics.

With the advent of high-performance computing (HPC) tools within the past decade, modeling and simulation have witnessed great advancement across a wide domain of disciplines including AM [10]. These models (often referred to as *computational models*) are used to analyze and understand a physical process through simulation, in contrast to solely relying on extensive and costly experimental trials. L-PBF is no exception and many research groups have invested significant time and resources to develop simulations models for L-PBF [4, 11–15].

The majority of computational models for L-PBF developed to date rely on principles of thermodynamics and heat transfer mechanics. Although extremely useful, this type of models typically involve some assumptions that aim to reduce their complexity and computational times. Consequently, it is well known that the simulation results from these computational models may deviate from the real process. Hence, verification and validation (V&V) for these models are required in order to draw valid conclusions and insights based on them [16].

The current work represents one of the first efforts to use Uncertainty Propagation (UP) analysis for validating computational models used in metal L-PBF. UP is an area within the broad field of uncertainty quantification (UQ) that focuses on characterizing the uncertainty in model response and predictions as a function of uncertainty in model inputs [17, 18].

We choose to conduct UP analysis to validate two different simulation models for L-PBF: a reduced order thermal model and a higher fidelity finite element thermal model (FETM). The first model was originally developed by Eagar and Tsai [19] for welding processes. The model considers a traveling heat source with a Gaussian profile on a flat metallic plate and calculates temperature distributions across the plate. For simplification, we refer to this model as the Eagar-Tsai (or ET) model hereafter. This model has been the baseline model of choice in several prior studies on L-PBF since it simulates the basic operation that takes place during the process (i.e., heat source scanning on a plate) and provides insight on the resulting thermal history. For instance, King et al. [5] uses the ET model to understand how melt pool characteristics behave based on a fractional factorial design of the inputs. Kamath [20] and King et al. [21] present a data-driven framework that employs the ET model to construct a predictive surrogate model. They use several sampling techniques such as random and best candidate sampling, along with decision trees surrogate models, and show how these data-driven approaches can be used in lieu of the actual ET model. Lastly, Kamath et al. [22] used ET model simulations and simple single-track experiments to guide parameter selection for building high-density L-PBF parts. Examples of other research studies that utilized ET model in domains other than AM include [23–25].

The second model is a finite element thermal model (FETM) developed by Karayagiz et al. [26]. In contrast to the ET model which models a heat source on a bare plate, this model considers a Gaussian-profile heat source on a layer of powder on top of a solid substrate. Finite element analysis models are very popular in modeling L-PBF processes (see for instance [27–30]).

Accepted Manuscript Not Copyedited

Downloaded From: http://biomechanical.asmedigitalcollection.asme.org/ on 09/04/2018 Terms of Use: http://www.asme.org/about-asme/terms-of-use

Journal of Manufacturing Science and Engineering. Received November 08, 2017;
Accepted manuscript posted August 17, 2018. doi:10.1115/1.4041179
Copyright (c) 2018 by ASME

The key contribution of the current work is addressing the literature gap related to the lack of systematic studies that conduct UP analysis for computational models used in L-PBF. More specifically, we employ for the first time a UP framework based on generalized Polynomial Chaos Expansions (gPCE) to the ET and FETM models in order to quantify the uncertainty in melt pool predictions as a function of uncertainty in process parameters that are input to the models. Next, we use the UP framework to validate these models using experimental measurements conducted on a commercial L-PBF system.

The paper is organized as follows: Section 2 presents a brief discussion of the current state of the art on L-PBF modeling and UP. Next, Section 3 presents the formal mathematical and statistical formulations for the UP framework that will be used to conduct UP analysis for the ET and FETM models in Section 4 and 5 respectively. The paper concludes by providing insights and directions for future research in Section 6.

2 State of the Art

Modeling and simulation of AM (in particular, L-PBF) processes have witnessed considerable advancement over the past decade, especially with concurrent advances in computational hardware and software, in addition to having been identified as a key research need to push the boundaries of AM in many recently published research roadmaps [10, 31, 32].

Many research groups have contributed to developing simulation models for L-PBF processes. A considerable proportion of prior works have focused on developing finite element models (FEM) to simulate different physical phenomena during AM (see for instance [12, 33, 34]). In particular, the emphasis has been placed on predicting the thermal history, melt pool characteristics, cooling rates, and temperature gradients. Other research groups with access to powerful computational resources have spent efforts to develop higher-fidelity models, through conducting more in-depth studies of the physical phenomena during the process and relaxing simplifying assumptions made in other models. Some of these models can be found in [4, 11, 35], which incorporate different aspects within the simulations such as: multi-scale modeling, powder particles mechanics, and 3D fluid flow.

Ongoing advances in the modeling and simulation of AM processes have not been matched with concurrent efforts to conduct systematic UQ of these models, with few exceptions (see for example [36, 37]). This is an important task, both for AM and for computer simulations models in the general sense, since almost all of these models involve layers and sources of uncertainty in their simulations and predictions [38]. As stated in Section 1, generalized Polynomial Chaos Expansions is the framework chosen to conduct UP analysis in the present study. This technique was first introduced by Wiener [39] in 1938, and has been applied to computer simulation models in other fields such as computational fluid dynamics [40–42], reliability engineering [43], and aerospace applications [44]. To the best of the authors' knowledge, there are no prior investigations that conduct formal UP analysis (including gPCE-based UP) to physics-based models for L-PBF processes. One recent work by Gorguluarslan et al. [45] has conducted UP analysis on a finite element model for simulating mechanical behavior of lattice scaffolds produced used AM. However, the work does not directly conduct the analysis on a model that simulates the AM process itself. The main contribution of the current work is conducting the first formal gPCE-based UP analysis for physics-based model that simulate aspects of AM processes; in particular we consider the Eagar-Tsai model which can be used to predict the thermal field during L-PBF processes.

3 Uncertainty Propagation Framework

Our proposed framework employs generalized Polynomial Chaos Expansions (gPCE) for propagation of uncertainty through the computational model. The building blocks of the framework include Elastic Nets regression to fit the gPCE model, and variance-based sensitivity analysis as a method to evaluate the influence of different inputs (or combination of inputs) on model outputs.

3.1 Generalized Polynomial Chaos Expansions

Before describing gPCE, it is useful to first briefly introduce Functional Chaos Expansions. This is a class of spectral methods developed by Wiener [39] capable of representing a probabilistic model as a simpler deterministic model while still capturing its randomness and uncertainty by reformulating it as a weighted infinite sum of basis functions. Following the formulations for gPCE by Blatman and Sudret [43], we define the probability space $(\Omega, \mathcal{F}, \mathcal{P})$ with sample space Ω, σ-algebra $\mathcal{F}$ and probability measure $\mathcal{P}$, and a deterministic model

$$y = \mathcal{M}(\mathbf{x}) \tag{1}$$

with $\mathbf{x} \in \mathcal{X} \subseteq \mathbb{R}^q$ and $y \in \mathbb{R}$. Input $\mathbf{x} = [x_1, \ldots, x_q]$ is represented as a realization from random vector $\mathtt{X}$ defined by its joint probability distribution function (pdf) $p_{\mathtt{X}}(\mathbf{x})$, with respective marginal pdfs, $p_{\mathtt{X}_i}(x_i) \forall i \in \{1, \ldots, q\}$. Given that $\mathtt{X}$ is random variable, it follows by Equation (1) that y is a realization of random variable $\mathtt{Y}$.

Downloaded From: http://biomechanical.asmedigitalcollection.asme.org/ on 09/04/2018 Terms of Use: http://www.asme.org/about-asme/terms-of-use

Journal of Manufacturing Science and Engineering. Received November 08, 2017;
Accepted manuscript posted August 17, 2018. doi:10.1115/1.4041179
Copyright (c) 2018 by ASME

In Functional Chaos Expansions, random input vector $\mathtt{X}$ is represented in a Hilbert space $\mathcal{L}_2(\Omega, \mathcal{F}, \mathcal{P})$ of square-integrable functions with respect to $p_{\mathtt{X}}(\mathbf{x})$, with the requirement of finite second moments:

$$\begin{aligned}\mathbb{E}\left[\mathtt{X}_i^2\right] &= \int_{\Omega} \mathtt{X}_i^2(\omega)\, d\mathcal{P}(\omega) \\ &= \int_{\mathcal{X}_i} x_i^2\, p_{\mathtt{X}_i}(x_i)\, dx_i \\ &< +\infty\end{aligned} \tag{2}$$

and thus *inner product* is defined as

$$\left\langle x_i, x_j \right\rangle_{\mathcal{L}_2} \equiv \mathbb{E}\left[\mathtt{X}_i \cdot \mathtt{X}_j\right] = \int_{\mathcal{X}} x_i x_j\, p_{\mathtt{X}}(\mathbf{x})\, d\mathbf{x} \tag{3}$$

Next, assuming that the model response $\mathtt{Y}$ also has finite variance, $\mathbb{E}\left[\mathtt{Y}^2\right] < +\infty$, response y can be written in a functional chaos representation, or in other words, as a converging series of known multivariate basis functions $\psi(\mathbf{x})$,

$$y = \mathcal{M}(\mathbf{x}) = \sum_{\alpha \in \mathbb{N}^q} a_\alpha \psi_\alpha(\mathbf{x}) \tag{4}$$

where a_α are unknown basis coefficients that are to be estimated, and α is a q-dimensional index set containing natural numbers $\mathbb{N}$, and will be explained in the next paragraphs.

When the basis functions $\psi(\mathbf{x})$ from Equation (4) are polynomial functions, the expansion is referred as a *Polynomial* Chaos Expansion. Within PCE framework, polynomials ψ must satisfy the following definitions:

Definition 1. For some $z \in \mathcal{Z} \subseteq \mathbb{R}$, a pair of different polynomials $P(z)$ and $Q(z)$ such that $P, Q : \mathcal{Z} \to \mathbb{R}$ are *orthogonal* to each other with respect to some weight function $w(z) > 0$ if and only if,

$$\langle P(z), Q(z) \rangle_{\mathcal{L}_2} = \int_{\mathcal{Z}} P(z)\, Q(z)\, w(z)\, dz = 0 \tag{5}$$

Definition 2. A polynomial P is *orthonormal* with respect to some weight function $w(z) > 0$, if it satisfies Definition 1 and its $\mathcal{L}_2$-norm is equal to 1:

$$\|P(z)\|_{\mathcal{L}_2} = \sqrt{\langle P(z), P(z) \rangle_{\mathcal{L}_2}} = 1 \tag{6}$$

The original expansion by Wiener [39] was formulated only for the case with independent and identically distributed (iid) standard Gaussian vector $\mathbf{x}$ and polynomials ψ of the Hermite sequence (or family)[1]. However, the approach has been studied further and subsequently extended to accommodate more probability distributions and polynomial families (i.e., Askey-scheme polynomials [46]), resulting in *generalized* Polynomial Chaos Expansions. Some of these orthonormal polynomial families include [44]:

- Legendre polynomials used with Uniform distributions between -1 and 1
- Hermite polynomials used with Standard Normal distributions
- Laguerre polynomials used with Gamma distributions
- Jacobi polynomials used with Beta distributions

Each of these families of orthonormal polynomials share the following recurrence relation relating any three consecutive terms in the sequence (within the same family),

$$\pi_j(z) = (a_j z + b_j)\, \pi_{j-1}(z) + c_j \pi_{j-2}(z) \tag{7}$$

[1] A sequence or a family of orthonormal polynomials imply the same meaning.

Accepted Manuscript Not Copyedited

Downloaded From: http://biomechanical.asmedigitalcollection.asme.org/ on 09/04/2018 Terms of Use: http://www.asme.org/about-asme/terms-of-use

Journal of Manufacturing Science and Engineering. Received November 08, 2017;
Accepted manuscript posted August 17, 2018. doi:10.1115/1.4041179
Copyright (c) 2018 by ASME

where $\pi_j(z)$ is a polynomial of degree $j \in \mathbb{N}$ (with initial cases $\pi_{-1}(z) = 0, \pi_0(z) = 1$) and coefficients a_j, b_j, c_j are uniquely defined for each family and for each polynomial degree j [47].

In the context of our original model $\mathcal{M}$, we define $\pi_j^{(i)}(x_i)$ to be a univariate polynomial of degree j. This polynomial satisfies Definitions 1 and 2 with respect to the marginal pdf of the ith input variable, $p_{\mathtt{X}_i}(x_i)$, for degrees j and k:

$$\begin{aligned}\left\langle \pi_j^{(i)}(x_i), \pi_k^{(i)}(x_i) \right\rangle_{\mathcal{L}_2} &= \mathbb{E}\left[\pi_j^{(i)}(\mathtt{X}_i) \cdot \pi_k^{(i)}(\mathtt{X}_i)\right] \\ &= \int_{\mathcal{X}_i} \pi_j^{(i)}(x_i)\, \pi_k^{(i)}(x_i)\, p_{\mathtt{X}_i}(x_i)\, dx_i \\ &= \delta_{j,k} \end{aligned} \tag{8}$$

where $\delta_{j,k}$ is the Kronecker delta that is equal to 1 when $j = k$ and 0 otherwise. Thus, $\pi_j^{(i)}(x_i)$ is an orthonormal polynomial.

Multivariate polynomials $\psi(\mathbf{x})$ are calculated by tensorizing all q univariate polynomials from every component of $\mathbf{x}$, thus

$$\psi_\alpha(\mathbf{x}) = \prod_{i=1}^{q} \pi_{\alpha_i}^{(i)}(x_i) \tag{9}$$

where index set $\alpha = \{\alpha_1, \ldots, \alpha_q\}$ is the set of indices that indicates the order for every univariate polynomial π that belongs to ψ, and hence in gPCE context, ψ are called basis functions.

In this application, it will be assumed that the inputs are statistically independent from each other, $p_{\mathtt{X}}(\mathbf{x}) = \prod_{i=1}^{q} p_{\mathtt{X}_i}(x_i)$, and thus, it can easily be demonstrated that $\psi(\mathbf{x})$ are also orthonormal multivariate polynomials:

$$\begin{aligned}\left\langle \psi_\beta(\mathbf{x}), \psi_\kappa(\mathbf{x}) \right\rangle_{\mathcal{L}_2} &= \mathbb{E}\left[\psi_\beta(\mathtt{X}) \cdot \psi_\kappa(\mathtt{X})\right] \\ &= \int_{\mathcal{X}} \psi_\beta(\mathbf{x})\, \psi_\kappa(\mathbf{x})\, p_{\mathtt{X}}(\mathbf{x})\, d\mathbf{x} \\ &= \delta_{\beta,\kappa} \end{aligned} \tag{10}$$

The case when dealing with statistically correlated inputs x_i's has also been demonstrated, however additional mathematical development that is outside the scope of this paper needs to be undertaken [43].

The objective is then to estimate the coefficients a_α in Equation (4), referred to as PC coefficients in the remainder of the paper. Different approaches can be followed to achieve this. We employ a *non-intrusive regression* method to build the gPCE model, since our focus is on computationally expensive models regarded as black boxes (most of the time we do not know or do not have access to modify governing equations and other relationships involved during simulations). The interested reader is referred to the following works for more details regarding the theory and selection of other different methods (such as *projection* techniques) [18, 43, 44].

In order to estimate the PC coefficients through the regression methodology, we need to gather data from model $\mathcal{M}$ by running several simulations at different combinations of values for input $\mathbf{x}$ to construct the gPCE model. We define an $n \times q$ input matrix $\mathbb{X}$ sampled from their corresponding probability distribution $p_{\mathtt{X}}(\mathbf{x})$ and an n-dimensional output vector $\mathbb{Y}$ as

$$\mathbb{X} = \begin{bmatrix} \mathbf{x}_1^\top \\ \vdots \\ \mathbf{x}_n^\top \end{bmatrix}, \; \mathbb{Y} = \mathcal{M}(\mathbb{X}) = \begin{bmatrix} y_1 = \mathcal{M}(\mathbf{x}_1) \\ \vdots \\ y_n = \mathcal{M}(\mathbf{x}_n) \end{bmatrix} \tag{11}$$

to represent the dataset that has been acquired through the model $\mathcal{M}$. Since the q columns of the matrix $\mathbb{X}$ typically have different units, we normalize the elements of the matrix to the unit hypercube $[0,1]^q$.

Additionally, to enable computation the series in Equation (4) is truncated to a default number t, which describes the maximum polynomial order allowed within the expansion,

$$y \approx \sum_{|\alpha| \leq t} a_\alpha \psi_\alpha(\mathbf{x}) \tag{12}$$

Accepted Manuscript Not Copyedited

Downloaded From: http://biomechanical.asmedigitalcollection.asme.org/ on 09/04/2018 Terms of Use: http://www.asme.org/about-asme/terms-of-use

Journal of Manufacturing Science and Engineering. Received November 08, 2017;
Accepted manuscript posted August 17, 2018. doi:10.1115/1.4041179
Copyright (c) 2018 by ASME

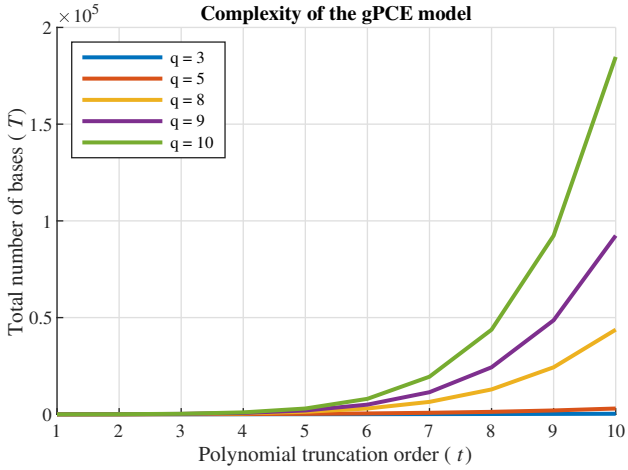

Figure 1. Computational complexity of the gPCE model based on values for t and q.

with $|\alpha| = \sum_{i=1}^{q} \alpha_i$. This truncation implies that there will be $T = \binom{t+q}{t}$ different basis functions $\psi(\mathbf{x})$ in the summation term in Equation (12).

Finally, after accounting for the whole dataset and writing the problem in matrix notation, we end up with a linear-regression type problem

$$\Psi(\mathbb{X})\,\mathbf{a} = \mathbb{Y} \tag{13}$$

where $\mathbf{a} = [a_{\mathbf{0}} \ldots, a_{\alpha}, \ldots]^{\top}_{|\alpha| \leq t}$ is the vector of PC coefficients and $\Psi(\mathbb{X})$ is a matrix of bases having the ith row equal to $[\psi_{\mathbf{0}}(\mathbf{x}_i) \ldots, \psi_{\alpha}(\mathbf{x}_i), \ldots]_{|\alpha| \leq t}$, and thus we are able to estimate the PC coefficients following any method for linear regression.

Selection of truncation order t is important since it defines the computational complexity of the model given the fact that it controls the number of basis functions present in the series in Equation (12) (denoted by T), and hence the number of columns in matrix $\Psi(\mathbb{X})$. It can be seen in Figure 1 that for truncation orders t lower than 5, the change in T is not significant for different dimensionalities of $\mathbf{x}$ (denoted by q). However, for truncation orders larger than or equal to 5, the value of T increases significantly.

Lastly, it is worth noting that the *null* index set

$$\alpha = \mathbf{0} = \{0, \ldots, 0\} \tag{14}$$

corresponds to the basis with degree zero for all univariate components, thus

$$\psi_{\mathbf{0}}(\mathbf{x}) = \prod_{i=1}^{q} \pi_0^{(i)}(x_i) = 1 \tag{15}$$

satisfies for any orthonormal family, and its corresponding PC coefficient is denoted as $a_{\mathbf{0}}$. In the next subsection we describe the technique employed for coefficient estimation.

3.2 Elastic Net Regularization

Given the linear model in Equation (12), the PC coefficients can be estimated following any standard technique such as Least Squares, Ridge Regression, Lasso Regression, Least Angle Regression, among many. Nevertheless, not all of these methods will work for all cases. For instance, if the number of datapoints n is less than T (the total number of basis functions), then ill-posed matrices will be present in the linear regression problem and techniques such as Least Squares or Ridge Regression might fail.

We choose to employ the more recent approach: Elastic Nets regularization developed by Zou and Hastie [48]. This technique involves a combination of Least Squares, Lasso and Ridge regression [49]. Consequently, the method uses both $\mathcal{L}_1$- and $\mathcal{L}_2$-norm to account for: sparsity in the model by variable selection without any limits on the number of selected variables (as opposed to Lasso), a strictly convex loss function with a unique minimum (with the inclusion of Ridge), and grouping of correlated variables (as opposed to Lasso that selects only one and ignore the rest).

Accepted Manuscript Not Copyedited

Downloaded From: http://biomechanical.asmedigitalcollection.asme.org/ on 09/04/2018 Terms of Use: http://www.asme.org/about-asme/terms-of-use

Journal of Manufacturing Science and Engineering. Received November 08, 2017;
Accepted manuscript posted August 17, 2018. doi:10.1115/1.4041179
Copyright (c) 2018 by ASME

The formulation for the Elastic Net regularization is as follows,

$$\hat{\mathbf{a}} = \arg\min_{\mathbf{a}\in\mathbb{R}^T} \left[\frac{1}{2n} \sum_{i=1}^{n} \left(y_i - \mathbf{a}^\top \boldsymbol{\psi}(\mathbf{x}_i) \right)^2 + \lambda \left(\frac{1}{2} (1-\gamma) \|\mathbf{a}_{-\mathbf{0}}\|_{\mathcal{L}_2}^2 + \gamma \|\mathbf{a}_{-\mathbf{0}}\|_{\mathcal{L}_1} \right) \right] \tag{16}$$

where $\mathbf{a}_{-\mathbf{0}} = \mathbf{a} \setminus a_{\mathbf{0}}$ is the set of all PC coefficients other than that one corresponding to the null indexed basis; λ and γ are regularization hyperparameters that are to be set prior to minimization. These hyperparameters are selected following a grid search algorithm based on a cross-validation metric as a measure of performance (see details in Section 4.3). This is a common approach in the Machine Learning community [50].

Additionally, norms in this context can be calculated following the general $\mathcal{L}_p$-norm,

$$\|\mathbf{a}_{-\mathbf{0}}\|_{\mathcal{L}_p} = \left(\sum_{0<|\alpha|\leq t} |a_\alpha^p| \right)^{1/p} \tag{17}$$

After estimating coefficients $\mathbf{a}$ through Equation (16), the non-intrusive gPCE regression method can be thought of as a fast data-driven surrogate for the model $\mathcal{M}$ based on the training data, through simply approximating it with Equation (12). The last remaining step now is to quantify uncertainty in the model response given uncertainty in model inputs using that surrogate.

3.3 Uncertainty Propagation using gPCE

Once the PC coefficients have been estimated, gPCE can be used to propagate uncertainty through the black-box model $\mathcal{M}$. It is important to note that this framework will not provide the probability density function for the model output in closed form, but will provide very useful information about its statistical moments.

The first moment, $\mathbb{E}[\mathrm{Y}]$, is calculated given the fact that $\boldsymbol{\psi}_{\mathbf{0}}(\mathbf{x}) = 1$ from Equation (15), and the inner product property for multivariate orthonormal polynomials from Equation (10), thus

$$\begin{aligned}
\mathbb{E}[\mathrm{Y}] &= \mathbb{E}[\mathrm{Y} \cdot \boldsymbol{\psi}_{\mathbf{0}}(\mathrm{X})] \\
&= \langle y, \boldsymbol{\psi}_{\mathbf{0}}(\mathbf{x}) \rangle_{\mathcal{L}_2} \\
&= \int_{\mathcal{X}} \left(\sum_{|\alpha|\leq t} a_\alpha \psi_\alpha(\mathbf{x}) \right) \boldsymbol{\psi}_{\mathbf{0}}(\mathbf{x})\, p_{\mathrm{X}}(\mathbf{x})\, d\mathbf{x} \\
&= \sum_{|\alpha|\leq t} \left[a_\alpha \int_{\mathcal{X}} \psi_\alpha(\mathbf{x})\, \boldsymbol{\psi}_{\mathbf{0}}(\mathbf{x})\, p_{\mathrm{X}}(\mathbf{x})\, d\mathbf{x} \right] \\
&= a_{\mathbf{0}}
\end{aligned} \tag{18}$$

Similarly, for the second moment, it follows that

$$\begin{aligned}
\mathbb{E}\left[\mathrm{Y}^2\right] &= \mathbb{E}[\mathrm{Y} \cdot \mathrm{Y}] \\
&= \langle y, y \rangle_{\mathcal{L}_2} \\
&= \int_{\mathcal{X}} \left(\sum_{|\alpha|\leq t} a_\alpha \psi_\alpha(\mathbf{x}) \right) \left(\sum_{|\alpha|\leq t} a_\alpha \psi_\alpha(\mathbf{x}) \right) p_{\mathrm{X}}(\mathbf{x})\, d\mathbf{x} \\
&= \sum_{|\alpha|\leq t} a_\alpha^2
\end{aligned} \tag{19}$$

Accepted Manuscript Not Copyedited

Downloaded From: http://biomechanical.asmedigitalcollection.asme.org/ on 09/04/2018 Terms of Use: http://www.asme.org/about-asme/terms-of-use

Journal of Manufacturing Science and Engineering. Received November 08, 2017;
Accepted manuscript posted August 17, 2018. doi:10.1115/1.4041179
Copyright (c) 2018 by ASME

and the variance of the output distribution equals to

$$\begin{aligned}\mathrm{var}\left[\mathrm{Y}\right] &= \mathbb{E}\left[\mathrm{Y}^2\right] - \mathbb{E}\left[\mathrm{Y}\right]^2 \\ &= \sum_{|\alpha|\leq t} a_\alpha^2 - a_{\mathbf{0}}^2 \\ &= \sum_{0<|\alpha|\leq t} a_\alpha^2 \end{aligned} \tag{20}$$

Further moments can be calculated following similar procedures [43]. It is worth mentioning that the formulation in this section is valid for the univariate case. That is, the model output $y \in \mathbb{R}$ is a scalar quantity.

3.4 Sensitivity Analysis

An important aspect in UQ is Sensitivity Analysis (SA), which deals with identifying which inputs (or combination of inputs) are influential to the response, and what the corresponding magnitudes of these influences are, relative to one another. We focus on Global SA and specifically on *variance-based* SA methods (also know as *Sobol indices*) since they provide a powerful framework to decompose the variance of the model output and attribute it to different inputs or sets of inputs [51].

Within our original problem setup, we maintain the assumption that model $\mathcal{M}$ is defined in the Hilbert space $\mathcal{L}_2(\Omega, \mathcal{F}, \mathcal{P})$, and takes inputs $\mathbf{x} = \{x_1, \ldots, x_q\} \in \mathcal{X} \subseteq \mathbb{R}^q$ that are statistically independent. Following formulations provided in Owen [51], we define the set of input indices $Q = \{1, \ldots, q\}$ and subset $u = \{j_1, j_2, \ldots, j_{|u|}\} \subseteq Q$, with cardinality $|u|$, to be a subset of input indices, with its complement set denoted as $-u \equiv Q \setminus u$. Hence, we can write inputs defined by u as $\mathbf{x}_u = \left\{x_{j_1}, \ldots, x_{j_{|u|}}\right\} \in \mathcal{X}_u \subseteq \mathcal{X}$.

Variance-based SA is based on *Analysis of Variance* (ANOVA) decomposition, where the model under study is decomposed into several functions that depend only on different input subsets,

$$y = \mathcal{M}(\mathbf{x}) = \sum_{u \subseteq Q} \mathcal{M}_u(\mathbf{x}) \tag{21}$$

with

$$\mathcal{M}_u(\mathbf{x}) = \int_{\mathcal{X}_{-u}} \mathcal{M}(\mathbf{x})\, d\mathbf{x}_{-u} - \sum_{v \subset u} \mathcal{M}_v(\mathbf{x}) \tag{22}$$

Under these settings, u is a set of factors and $\mathcal{M}_u$ is the corresponding effect in the model. If $|u| = 1$ then $\mathcal{M}_u$ is called main effect for input x_j. Otherwise, if $|u| > 1$, then $\mathcal{M}_u$ is known as the interaction among all x_j for all $j \in u$.

The complete ANOVA decomposition will have $2^q - 1$ different $\mathcal{M}_u$, and yields the following result:

$$\begin{aligned}\sigma^2 &= \mathrm{var}\left[\mathcal{M}(\mathrm{X})\right] \\ &= \sum_{u \subseteq Q} \sigma_u^2 \end{aligned} \tag{23}$$

where $\sigma_u^2 = \int_{\mathcal{X}_u} \mathcal{M}_u(\mathbf{x})^2\, d\mathbf{x}_u$ is the single effect (or partial variance) for u. For a more detailed discussion, the reader is referred to [51].

Sobol indices are hence defined as

$$\overline{\tau}_u^2 = \sum_{v \cap u \neq \emptyset} \sigma_v^2 \tag{24}$$

$$\underline{\tau}_u^2 = \sum_{v \subseteq u} \sigma_v^2 \tag{25}$$

where $\overline{\tau}_u^2$ is called *total sensitivity index*, which counts every ANOVA component that includes at least one element of set u, and $\underline{\tau}_u^2$ is called *closed sensitivity index*, which is the sum of the variance components for set u and all of its subsets. If $\underline{\tau}_u^2$ is

Accepted Manuscript Not Copyrighted

Downloaded From: http://biomechanical.asmedigitalcollection.asme.org/ on 09/04/2018 Terms of Use: http://www.asme.org/about-asme/terms-of-use

Journal of Manufacturing Science and Engineering. Received November 08, 2017;
Accepted manuscript posted August 17, 2018. doi:10.1115/1.4041179
Copyright (c) 2018 by ASME

large, then subset u is important, or if $\bar{\tau}_u^2$ is small, then subset u is not important [51]. These indices satisfy $\underline{\tau}_u^2 + \bar{\tau}_{-u}^2 = \sigma^2$, and are usually presented as normalized quantities, $\frac{\bar{\tau}_u^2}{\sigma^2}$ and $\frac{\underline{\tau}_u^2}{\sigma^2}$.

An attractive feature in gPCE is that Sobol indices can be easily calculated as by-products of the procedure, after some adaptation [52]. The gPCE-based ANOVA decomposition (with truncation) is

$$y \approx \sum_{u \subseteq Q} \sum_{\alpha \in \alpha_u} a_\alpha \psi_\alpha(\mathbf{x}) \tag{26}$$

where $\alpha_u = \{\alpha \colon \alpha_j > 0 \; \forall j \in u,\ \alpha_k = 0 \; \forall k \notin u, \text{ and } |\alpha| \leq t\}$ which activates those bases that depend only on the inputs indexed by set u.

Therefore, given the orthonormality property of polynomials ψ, Sobol indices are calculated as follows:

- gPCE single effect index

$$\sigma_{\mathrm{PC},u}^2 = \sum_{\alpha \in \alpha_u} a_\alpha^2 \tag{27}$$

- gPCE-based closed sensitivity index

$$\underline{\tau}_{\mathrm{PC},u}^2 = \sum_{v \subseteq u} \sum_{\alpha \in \alpha_v} a_\alpha^2 \tag{28}$$

- gPCE-based total sensitivity index

$$\bar{\tau}_{\mathrm{PC},u}^2 = \sum_{\alpha \in \alpha_u} a_\alpha^2 \tag{29}$$

with the difference that $\alpha_u = \{\alpha \colon \alpha_j > 0 \; \forall j \in u \text{ and } |\alpha| \leq t\}$ in this case.

These sensitivity indices are computed at minimal additional cost, since they only depend on PC coefficients that were already estimated in the previous subsection, which is the step that represents most of the computational cost within the whole framework. In fact, as the formulation suggests, these indices are calculated by simply adding coefficients after proper indexing and selection (actions that involve only elementary mathematical and logical operations), thus not incurring additional computational burden.

In the next sections, the complete UP methodology is applied into two different case studies for Additive Manufacturing computational models.

4 Case Study 1: UP-based Validation of the Eagar-Tsai model

The case study in this section will present a useful application for the proposed gPCE UP framework presented in Section 3: validating a computational model used in L-PBF metal AM process. First, we start by providing a quick overview to familiarize the reader with the model. Next, we present the detailed implementation of the UP to validate the model.

4.1 Overview of the Eagar-Tsai Model

The Eagar-Tsai model is an analytical thermal model developed by Eagar and Tsai [19] which calculates temperature fields associated with a traveling Gaussian-distributed heat source on a semi-infinite plate employing dimensionless mathematical reductions. The model was originally developed for melt pool analysis and prediction in welding processes. Since metal-based L-PBF AM can be thought of as a repetitive micro-welding process, this model has been very common for conducting some preliminary melt pool analysis in L-PBF [5, 20–22].

The model takes two main groups of inputs:

- Heat Source parameters: net heat input per unit time P, travel speed v, and parameter D describing the heat source profile.
- Material parameters: thermal conductivity k, specific heat capacity c_p, density ρ, and absorptivity A.

Accepted Manuscript Not Copyedited

Downloaded From: http://biomechanical.asmedigitalcollection.asme.org/ on 09/04/2018 Terms of Use: http://www.asme.org/about-asme/terms-of-use

Journal of Manufacturing Science and Engineering. Received November 08, 2017;
Accepted manuscript posted August 17, 2018. doi:10.1115/1.4041179
Copyright (c) 2018 by ASME

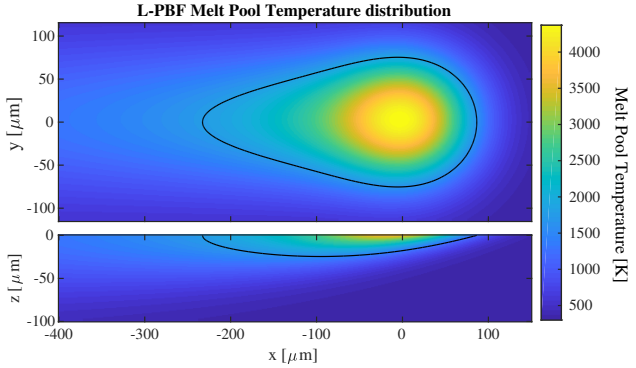

Figure 2. Example of the thermal field solution after simulation of the ET model, with a black contour line added at melting temperature. Plane xy shown at level $z = 0$, and plane xz shown at level $y = 0$.

Since our interest is on L-PBF processes, the analogous heat source parameters that we will deal with are: power of the laser beam P, scanning speed v, and gaussian-distributed laser beam diameter[2] $D4$.

An example of a solution (or model output) provided by the ET model is presented in Figure 2, in which a simulation was run with the following laser parameters $P = 200\,\mathrm{W}$, $v = 2.5\,\mathrm{m/s}$, $D4 = 100\,\mu\mathrm{m}$, and 430F Stainless Steel as the material system for the plate.

The model is important and relevant to the L-PBF process since it is a starting point in understanding the interaction between a moving heat source (the laser beam) onto a metal substrate plate, and the corresponding thermal phenomena behavior that occur. In other words, it is considered and used in many previous research efforts as a first approximation of the basic operating principle of L-PBF, despite the fact that it does not include melting of powder particles.

One further justification for choosing the ET model in this study: it follows an analytical solution, hence it is a simulation model that does not require extensive computational resources. It thus represents an excellent environment to demonstrate, validate and benchmark our proposed UP framework. It is very important to point out, however, that the proposed framework is most valuable in conducting UP analysis for other computational-intensive high-fidelity AM models, such as FEM. Since the simulation model is treated as a black-box in our non-intrusive gPCE framework, the framework is readily applicable to such high fidelity models.

4.2 Applicability of the gPCE-based UP Framework

Consider the following situation: in building a part using L-PBF, the operator sets nominal values for the processing parameters (for example, set the laser power P to 200 watts). In many existing commercial L-PBF systems, the actual realized values of the processing parameters might deviate from the nominal values set by the user. This has often been identified as one possible reason for the low repeatability of L-PBF parts (and metal AM parts in general). Currently, it is generally assumed that the actual values of the processing parameters would exhibit some degree of uncertainty around their nominal set values. The question to be addressed is thus: how does uncertainty in the processing parameters affect uncertainty in the properties of the fabricated part?.

UP analysis can be used to answer this question. We conduct experiments on a ProX 100 DMP L-PBF system by 3D Systems. The system is equipped with a fiber laser beam having a Gaussian profile and wavelength $\lambda = 1070\,\mathrm{nm}$, beam diameter of approximately $70\,\mu\mathrm{m}$, a maximum laser beam power of $50\,\mathrm{W}$. Builds are conducted under an Argon inert protective atmosphere. We choose the melt pool *width* as the quantitative metric on which the answer to the question will be based. We acknowledge that other metrics, such as the melt pool depth, are also important metrics. However, the melt pool width was selected for this particular study since the main focus is on demonstrating the uncertainty propagation framework, which can readily be applied to any other metric deemed relevant by the user. One motivation for selecting the melt pool width as a metric is the relative simplicity of experimentally measuring it in contrast to other metrics that are frequently used, such as melt pool depth which necessitates sectioning the build substrate and conducting chemical etching, or melt pool temperature which poses even more challenges to experimentally capture.

More specifically, we will assume that there is uncertainty in the laser processing parameters (P, v, $D4$). It should be noted that these three selected parameters are assumed to be statistically independent. Next, experimental measurements of the melt pool width from single-track scans on a bare metallic substrate plate will be compared with the results from the gPCE UP framework applied to the ET model. In running the ET model, we will use 430F Stainless Steel as the material system to be consistent with the substrate plates used on ProX 100 DMP. The material properties are given by [53]: $k = 26.3\,\mathrm{W/m{\cdot}K}$, $c_p = 0.46\,\mathrm{J/g{\cdot}K}$, $\rho = 7.8\,\mathrm{g/cm^3}$, $A = 0.3$, and a melting point of $T_m = 1460\,\mathrm{K}$.

[2]The distance equivalent to 4 standard deviations of the Gaussian profile of the beam (usually denoted as $D4\sigma$ in other studies).

Accepted Manuscript - Not Copyedited

Downloaded From: http://biomechanical.asmedigitalcollection.asme.org/ on 09/04/2018 Terms of Use: http://www.asme.org/about-asme/terms-of-use

Journal of Manufacturing Science and Engineering. Received November 08, 2017;
Accepted manuscript posted August 17, 2018. doi:10.1115/1.4041179
Copyright (c) 2018 by ASME

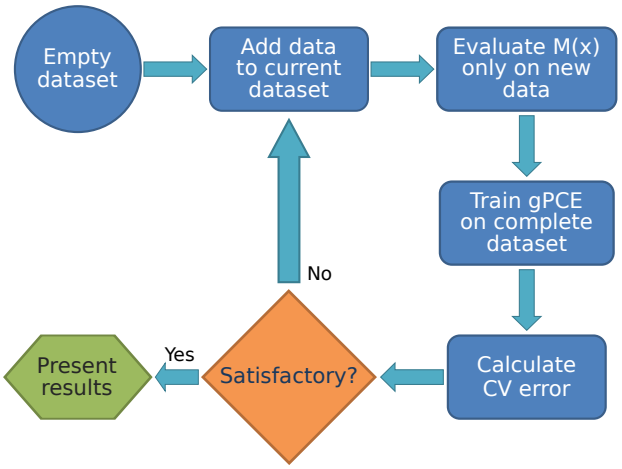

Figure 3. Sparse gPCE with adaptive sampling flow chart.

4.3 Implementing the UP Framework

4.3.1 Generalized Polynomial Chaos Expansions

Recall that our objective is to study how variations (even ones small in magnitude) around set nominal values of the processing parameters influence the melt pool characteristics. We set the nominal values of the processing parameters based on the system manufacturer recommendation in addition to our domain knowledge from previous processing of other stainless steel alloys (in particular 17-4 PH and 316L stainless steel alloys), and use the following probability distributions:

- Laser power: nominal at 49 W, assumed to follow a normal distribution with the following mean and variance: $P\,[\mathrm{W}] \sim N\left(49, 0.5^2\right)$.
- Scanning speed: nominal at $0.15\,\mathrm{m/s}$, assumed to follow a uniform distribution: $v\,[\mathrm{m/s}] \sim U\,(0.10, 0.20)$.
- Laser beam diameter: nominal at $70\,\mu$m, assumed to follow a uniform distribution: $D4\,[\mu\mathrm{m}] \sim U\,(70, 100)$.

These distributions are selected based on expert domain knowledge of the commercial L-PBF system on which validation experiments will be conducted as follows:

- The effective laser power delivered to the raw metal powder is assumed to be uncertain, centered around its nominal value, due to fluctuations in the power source to the laser system, accumulation of errors in laser optics, irregular powder morphology, or obstruction of the laser path due to spatter or plume. Due to the multiple sources that contribute to the uncertainty in laser power, a normal distribution is reasonable to model this uncertainty.
- The laser scanning speed is driven by a system comprised of mirror galvanometers, thus the ability of the system to achieve any desired speed is dependent on motor controllers, inertia and momentum of the mirrors, and the state of the system (e.g. deterioration or bad encoder reads from the system). The selected non-informative uniform distribution assumes that no further information regarding the distribution of the laser scanning speed is known beyond the upper and lower bounds.
- The laser beam diameter has been reported by the original equipment manufacturer (OEM) to be between 70 and $100\,\mu$m. Accordingly, a non-informative uniform distribution between these values has been assigned to this parameter.

A *sparse* gPCE with an *adaptive sampling* methodology is used to conduct the UP framework. In this methodology, we iteratively sample a batch of datapoints to fit the gPCE model until some target metric is met. Specifically, in each iteration we sample a number of datapoints from their corresponding distributions, fit the non-intrusive regression-based gPCE model[3], assess its performance through formal cross validation, and based on a set value for cross validation error target (set by the user), either a new iteration is run if the target was not met, or the procedure is successfully finished since the target has been met. Figure 3 schematically displays a flow chart of the methodology.

The methodology was first introduced by Blatman and Sudret [43], however in the present work a different technique for sparsity has been utilized. Our proposed method is *sparse* since the Elastic Nets regularization involves a variable selection step as part of the procedure, which identifies some bases as insignificant and set their corresponding PC coefficients at zero. Additionally, it is *adaptive* since it samples additional data depending on whether the model has not met the cross validation target with the current provided dataset. That is, it continues to adaptively add new information in a step-by-step fashion, in contrast to classical samples procedures where a single dataset is employed with fixed number of design points set *a priori*.

The procedure was implemented with the following criteria:

[3]In this step, a grid search algorithm is executed to find the best combination of the hyperparameters λ and γ.

Downloaded From: http://biomechanical.asmedigitalcollection.asme.org/ on 09/04/2018 Terms of Use: http://www.asme.org/about-asme/terms-of-use

Journal of Manufacturing Science and Engineering. Received November 08, 2017;
Accepted manuscript posted August 17, 2018. doi:10.1115/1.4041179
Copyright (c) 2018 by ASME

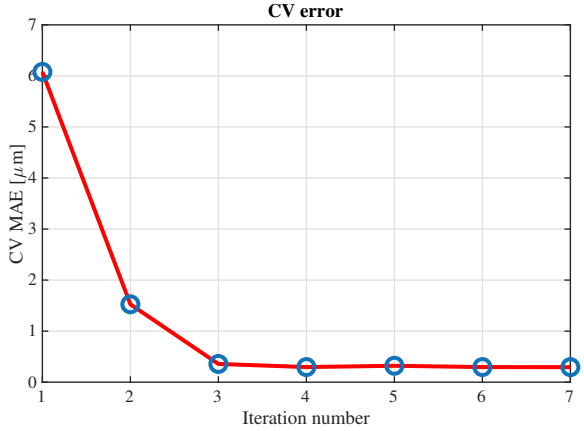

(a)

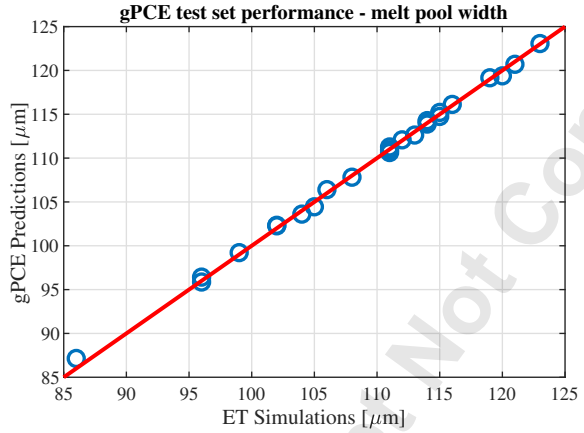

(b)

Figure 4. Performance of the sparse gPCE adaptive sampling algorithm. **a)** CV error history after 7 iterations showing convergence. **b)** Performance of the gPCE model over a test set.

- Each iteration adds 10 new datapoints to the dataset sampled from a scrambled Sobol's quasi-random uniform sequence generator [54], and then converted to their corresponding probability distributions. This number is selected to strike a balanced trade-off between computational burden of running new simulations and providing new information to the gPCE model.
- Model performance is measured using 10-fold Cross Validation (CV) with *mean absolute error* (MAE) as metric:

$$\text{MAE} = \frac{1}{n}\sum_{i=1}^{n}\left|Y_i^{(\text{ET})} - Y_i^{(\text{gPCE})}\right| \tag{30}$$

- Error target is set to $0.50\,\mu$m since we are using melt pool width as model metric, or until convergence has been achieved.
- Polynomial truncation is set at $t = 4$.

After executing the framework in Figure 3, the algorithm achieved the cross validation target after 7 iterations, which translates to 70 total simulations of the ET model, with a total execution time of 48 minutes. The algorithm stopped since it achieved convergence in CV error as shown in Figure 4a.

An extra validation step was further implemented, in which 25 new datapoints were sampled and evaluated with the ET model. This set of 25 new datapoints represented a *test dataset*, and was then compared to the predictions obtained using the gPCE model as shown in Figure 4b. An error of MAE $= 0.2997\,\mu$m was achieved, corroborating the good performance of the model over datapoints not previously used for training.

4.3.2 Sensitivity Analysis

Both the gPCE-based normalized single effect Sobol indices and the total sensitivity indices were computed (see Figure 5). Recall that while the objective of UP analysis is to quantify the uncertainty in model output given uncertainty in

Accepted Manuscript Not Copyedited

Downloaded From: http://biomechanical.asmedigitalcollection.asme.org/ on 09/04/2018 Terms of Use: http://www.asme.org/about-asme/terms-of-use

Journal of Manufacturing Science and Engineering. Received November 08, 2017;
Accepted manuscript posted August 17, 2018. doi:10.1115/1.4041179
Copyright (c) 2018 by ASME

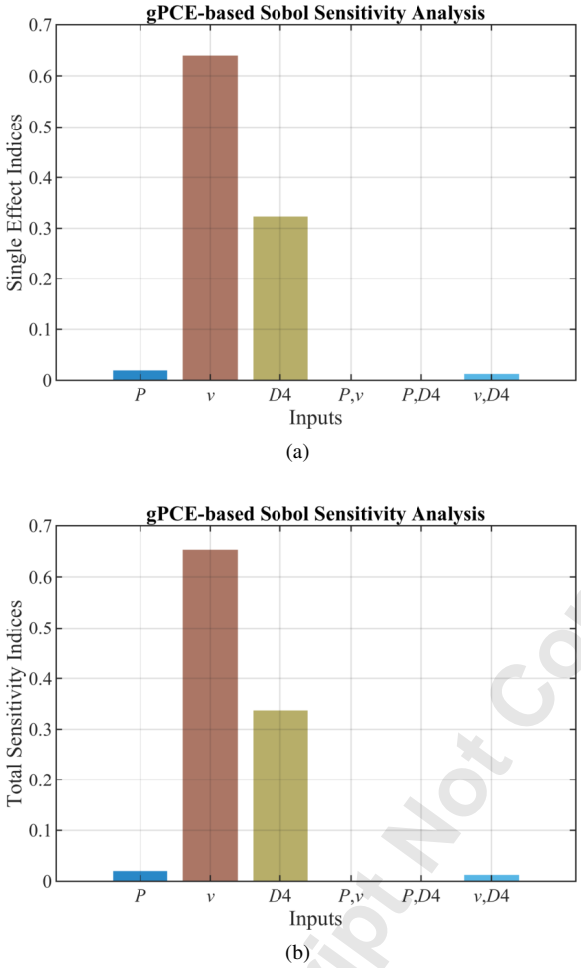

Figure 5. gPCE-based global sensitivity analysis. **a)** Normalized single effect and two-way interaction indices. **b)** Normalized Total Sensitivity indices.

model input(s), the complementary objective of sensitivity analysis is to assess the influence of a model input (or group of inputs) on the model output. Some uncertainty quantification approaches call for starting with sensitivity analyses first to identify which set of inputs will be included in a UP analysis. In other cases, the user might be already interested in a specific set of inputs (e.g. based on domain knowledge), as is the case with the current work. From Figure 5, it can be seen that both types of indices yield very similar values. This expected given the fact that in the elastic nets regularization step, many bases were deemed as non-important and their corresponding PC coefficients were set to zero. The remaining "active" bases were attributed with more influence over the model, and therefore contributing with more variance over the output.

Additionally, the results indicate that the laser scanning speed is the most influential input in our particular analysis, followed by laser beam diameter. An interesting, and somewhat unexpected, observation is that laser power is not recognized as very influential. This may confirm that some low uncertainty (represented by a low value of the standard deviation on the distribution of laser power) can be tolerated. The same does not hold true in the case of scanning speed or laser beam diameter.

4.3.3 Validation of UP Results through the Monte Carlo Method

We now conduct some further investigations to validate the results of the proposed UP framework. More specifically, we: (1) benchmark the results of the frameworks against the standard UP approach using Monte Carlo (MC) methods, and (2) compare our computational results with experimental measurements, in the two following sub-sections.

After training the gPCE model in Section 4.3, we determine statistical moments of the output distribution following Equations (18) and (20). We re-computed the statistical moments via brute force MC. Notice that while MC is generally the most common approach to conduct UP analysis, it is not a practical approach when computationally expensive models are being analyzed. This represents one more justification for our choice of the ET model in this study: since the ET model is reasonable in terms of computational burden, we were able to conduct standard MC analysis so we can use it to benchmark our proposed framework.

Accepted Manuscript Not Copyedited

Downloaded From: http://biomechanical.asmedigitalcollection.asme.org/ on 09/04/2018 Terms of Use: http://www.asme.org/about-asme/terms-of-use

Journal of Manufacturing Science and Engineering. Received November 08, 2017;
Accepted manuscript posted August 17, 2018. doi:10.1115/1.4041179
Copyright (c) 2018 by ASME

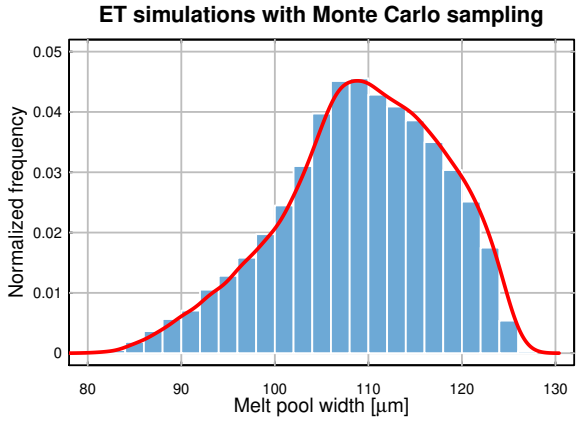

Figure 6. Histogram with a kernel density estimate (red line) after 15,000 ET simulations from MC random sampling.

Table 1. Melt pool width statistical distribution moments.

Method	Mean [μm]	Std. Dev. [μm]	Number of Datapoints
gPCE	109.3937	8.4744	70
MC	109.4061	8.5766	15,000

In the MC implementation, 15,000 datapoints were sampled from the input distributions and evaluated using the ET model on the Texas A&M 862-node Intel x86-64 Linux cluster supercomputer. The complete histogram of the validation dataset is shown in Figure 6.

Statistical moments based on gPCE and MC are presented in Table 1. It can be seen that the gPCE model first moment (mean) and second moment (represented by the standard deviation) are within 0.01% from the moments computed using brute force MC. However, the latter required more data samples than gPCE, with a factor of approximately 200. In other words, the gPCE framework yielded similar results to MC, but with a small fraction of computational time. The computational saving offered by gPCE will be even much more when an expensive computational model is involved.

4.3.4 Experimental Validation of the ET model

Once we have characterized the uncertainty in the ET simulation model for L-PBF processes, we want to validate it with real experimental data. In order to do this, we printed single tracks on a solid 430F stainless steel substrate at laser settings $P = 49\,\mathrm{W}$ and $v = 0.15\,\mathrm{m/s}$, and observed them under an optical microscope to measure the width of these tracks. An image of one of the samples is presented in Figure 7a, while a representation of the experimental data distribution through a box plot is illustrated in Figure 7b.

Model validation through UP is not a new procedure and has been investigated in several prior works. We follow a hypothesis testing method similar to the one previously used in [55, 56]: for a given confidence interval $100 \times (1-\alpha)\,\%$ at a specific significance level α, we compare measurements from physical experiments with simulation model predictions. If experimental measurements fall within the distribution of the results obtained from the simulation model, we reject the null hypothesis that the simulation model is not consistent with experimental results at that level of significance.

First, we transform the MC data using a Box-Cox power transformation [57]

$$Z = \begin{cases} \frac{y^{\kappa}-1}{\kappa} & \text{if } \kappa \neq 0 \\ \log(y) & \text{if } \kappa = 0 \end{cases} \tag{31}$$

with parameter $\kappa = 3$ (estimated via log-likelihood maximization). Next, we scale the transformed data down to a standard normal distribution (zero mean and unit variance), and assess the validity of the model with significance $\alpha = 0.05$.

Figure 8 displays the results for this experimental validation. The blue histogram represents the 15,000 ET simulations sampled from MC after Box-Cox transformation and standardization (i.e., mean 0 and variance 1), and the red curve is a kernel density estimate of the histogram data. Next, we approximate the gPCE results (first and second statistical moments)

Downloaded From: http://biomechanical.asmedigitalcollection.asme.org/ on 09/04/2018 Terms of Use: http://www.asme.org/about-asme/terms-of-use

Accepted Manuscript Not Copyedited

Journal of Manufacturing Science and Engineering. Received November 08, 2017;
Accepted manuscript posted August 17, 2018. doi:10.1115/1.4041179
Copyright (c) 2018 by ASME

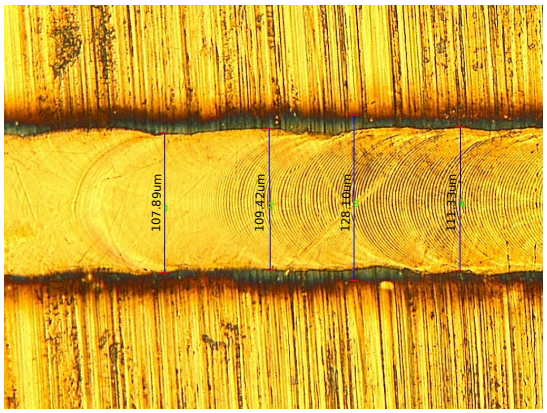

(a)

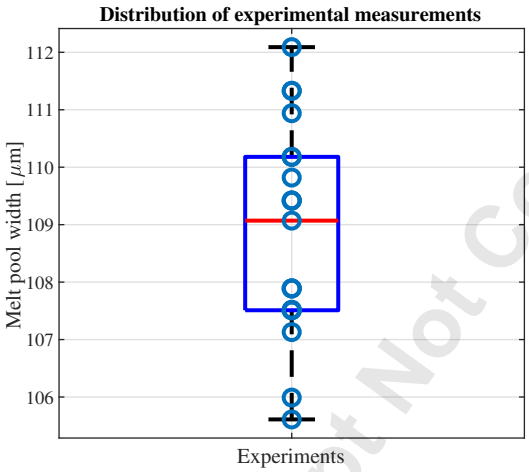

(b)

Figure 7. Experimental measurements of single tracks on a 430F Stainless Steel bare plate. **a)** Optical microscopy image. **b)** Dataset distribution.

to a Normal distribution, which after standardization becomes the standard Normal pdf represented by the yellow curve. It can be seen that both curves approximate each other well, reiterating the validity of the gPCE framework.

Additionally on Figure 8, the dashed vertical black lines represent the confidence interval at significance level $\alpha = 5\%$, while the purple circles represent the experimental observations under optical microscopy of the melt pool width after respective transformation and standardization (the position of the experimental observations on the vertical axis is solely for visual comparison within the histogram). It is clear that experiments are within the distribution of simulation results, and therefore we reject the null hypothesis that the ET model is not consistent with experimental results at 5% level of significance.

5 Case Study 2: UP-based Validation of a Finite Element Thermal Model

We conduct the UP-based validation for a higher fidelity finite element thermal model for L-PBF developed by Karayagiz et al. [26].

5.1 Overview of the FETM model

The FETM model was implemented in Comsol Multi-physics to study melt pool characteristics, including geometry and thermal profiles, during L-PBF. In this model, the powder layer is modeled as a a porous continuum medium over a thick solid substrate. Furthermore, it it accounts for several heat transfer mechanisms that take place during manufacturing such as conduction, convection, radiation, phase transitions[4], latent heat of melting/evaporation, temperature-dependent material properties, effective thermo-physical properties for the powder layer, and heat loss due to evaporation.

[4]Both, solid-to-liquid and liquid-to-gas transitions.

Accepted Manuscript Not Copyedited

Downloaded From: http://biomechanical.asmedigitalcollection.asme.org/ on 09/04/2018 Terms of Use: http://www.asme.org/about-asme/terms-of-use

Journal of Manufacturing Science and Engineering. Received November 08, 2017;
Accepted manuscript posted August 17, 2018. doi:10.1115/1.4041179
Copyright (c) 2018 by ASME

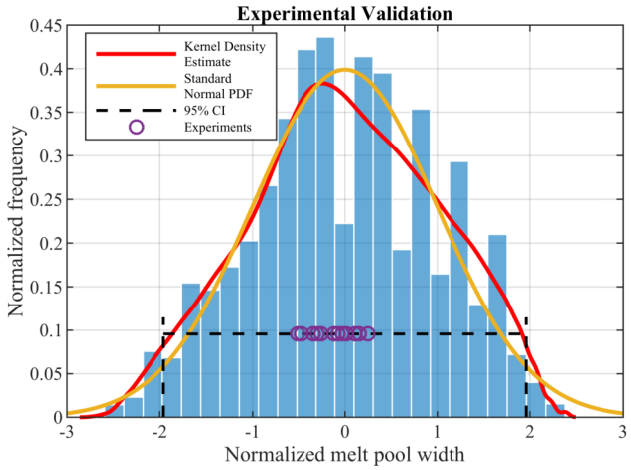

Figure 8. Experimental validation of the ET model via UP.

Table 2. Melt pool width statistical moments based on FEM model and gPCE.

Method	Mean [μm]	Std. Dev. [μm]	Number of Datapoints
gPCE	162.6085	10.3079	80

5.2 Implementing the UP Framework

5.2.1 Generalized Polynomial Chaos Expansions

Due to the physics incorporated in the model, the computational complexity is significantly higher than the ET model, and thus Monte Carlo-based analyses quickly become infeasible. The same procedure as presented in Section 4.3 is conducted for this model with the following specifications:

- Material system: Ti-6Al-4V.
- The powder layer thickness:30 μm, based on the original equipment manufacturer (OEM) recommendation.
- Laser power: nominal value of 49 W, and assumed to follow a normal distribution with $P\,[\mathrm{W}] \sim N\left(49, 0.5^2\right)$.
- Laser Scanning speed: nominal value of 0.107 $^{\mathrm{m}}/_{\mathrm{s}}$, following a uniform distribution: $v\,[^{\mathrm{m}}/_{\mathrm{s}}] \sim U\left(0.075, 0.125\right)$. Note that this is a different setting compared to Stainless Steel.
- Laser beam diameter: nominal value of 70 μm, following a uniform distribution: $D4\,[\mu\mathrm{m}] \sim U\left(70, 100\right)$.
- The sparse adaptive gPCE framework is applied under the same settings: each iteration adds 10 new datapoints, mean absolute error (MAE) is used as a cross validation metric, error target is 50 μm, and polynomial truncation order is set at $t = 4$.

After executing the framework, the algorithm reached the error target in the 5th iteration and achieved convergence at the 8th iteration, which translates to 80 total simulations of the FETM model. This is visually depicted in Figure 9a. The total execution time was approximately 2 weeks on a supercomputer, with an average time per simulation of 4 hours. The results for the statistical moments of melt pool width based resulting from the gPCE framework are presented in Table 2.

5.2.2 Sensitivity Analysis

Global sensitivity analysis indices based on gPCE were also calculated with single effect indices shown in Figure 9b. The plot shows a similar result to the ET model regarding the scanning speed and laser beam diameter being the most influential parameters influencing melt pool width. However, uncertainty in the laser beam diameter is found to account for the most influence in the melt pool width uncertainty while scanning speed is identified as the second most significant factor. Therefore, the same conclusion after sensitivity analysis of the ET model still holds true since it can be understood that a small change of a few watts in laser power can be tolerated, as opposed to a change of a few micrometers in laser beam diameter.

5.2.3 Experimental Validation of the thermal FEM model

To experimentally validate the FEM model, several single tracks were printed in Ti-6Al-4V for both powder and substrate plate at laser settings $P = 49$ W and $v = 0.107$ $^{\mathrm{m}}/_{\mathrm{s}}$. The powder layer was set to 30 μm. The width of the single tracks

Accepted Manuscript Not Copyedited

Downloaded From: http://biomechanical.asmedigitalcollection.asme.org/ on 09/04/2018 Terms of Use: http://www.asme.org/about-asme/terms-of-use

Journal of Manufacturing Science and Engineering. Received November 08, 2017;
Accepted manuscript posted August 17, 2018. doi:10.1115/1.4041179
Copyright (c) 2018 by ASME

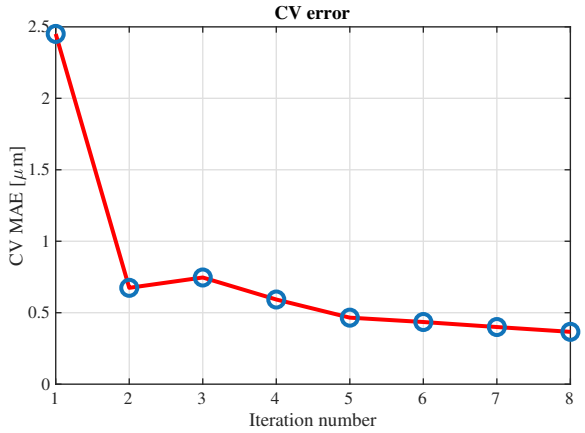

(a)

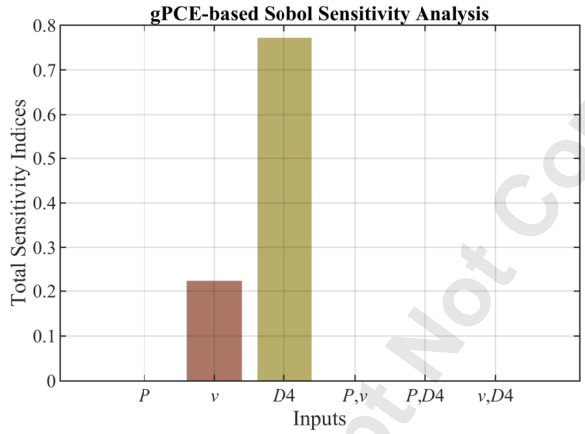

(b)

Figure 9. Application of the sparse and adaptive gPCE framework to the FEM model. **a)** CV error path after 8 iterations. **b)** gPCE-based sensitivity analysis showing normalized single effect and two-way interactions Sobol indices.

was measured using an optical microscope. One of these tracks can be seen in Figure 10a while the the distribution of the entire experimental dataset is shown in the box plot in Figure 10b.

Finally, we follow the same hypothesis testing method where the null hypothesis to be tested is that the FETM simulation model is not consistent with the experimental results. Figure 11 visually presents the results of the experimental validation after data standardization. In this case, it can be seen that most of the experimental measurements (red circles) are within the 95% confidence interval (black dashed lines) of the melt pool width distribution calculated by gPCE (and standardized, hence the standard normal distribution on the blue line). Hence, the null hypothesis is rejected at significance level $\alpha = 5\%$.

6 Conclusions

Although modeling and simulation of L-PBF AM processes has witnessed considerable advancement over the past decade, efforts to systematically quantify the uncertainties associated with these models have not been on par. In the present work, we employed an Uncertainty Propagation (UP) framework based on generalized Polynomial Chaos Expansions (gPCE) for two thermal models used in L-PBF (the Eagar-Tsai model and a finite element thermal model). The framework characterizes the uncertainty in the response of the models given uncertainty associated with the input model parameters. Specifically, we account for uncertainties in process parameters (laser power, scanning speed, laser beam diameter), and quantify their influence on the melt pool width. The implications of this paper are summarized as follows: (1) it represents one of the first efforts conducting formal UP analysis for physics-based models that model L-PBF processes, and (2) it can be used to answer practical questions related to the effect of uncertainty in some of the processing parameters in commercial AM systems (such as laser power or beam diameter) on melt pool characteristics, which is an important metric correlated with the quality of fabricated parts, (3) it is used to conduct validation of computational models for L-PBF.

The UP framework includes construction of the gPCE model through a non-intrusive regression method and Elastic Nets regularization, and sensitivity analysis to identify model parameters with most significant impact on the melt pool width. The implementation of the UP framework also involves an iterative procedure that consists of adaptively selecting simulation

Accepted Manuscript Not Copyedited

Downloaded From: http://biomechanical.asmedigitalcollection.asme.org/ on 09/04/2018 Terms of Use: http://www.asme.org/about-asme/terms-of-use

Journal of Manufacturing Science and Engineering. Received November 08, 2017;
Accepted manuscript posted August 17, 2018. doi:10.1115/1.4041179
Copyright (c) 2018 by ASME

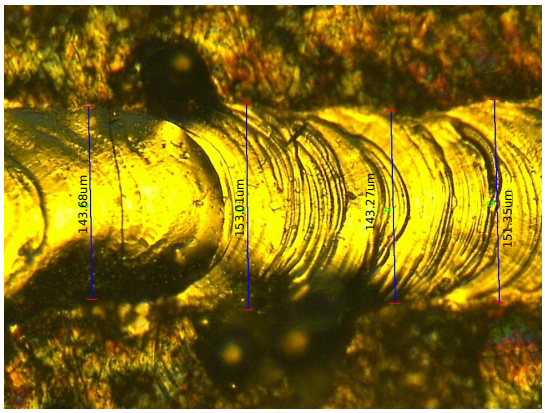

(a)

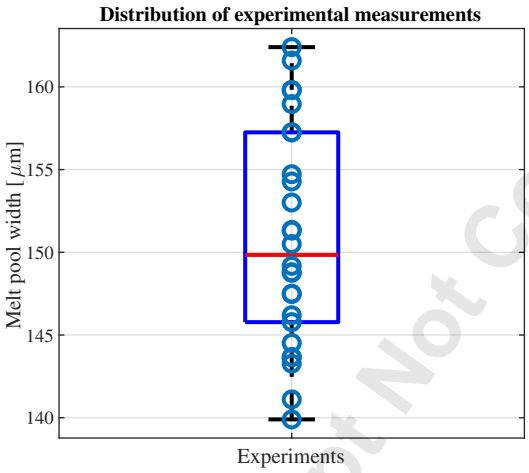

(b)

Figure 10. Experimental measurements of Ti-6Al-4V single tracks. **a)** Optical microscopy image. **b)** Dataset distribution.

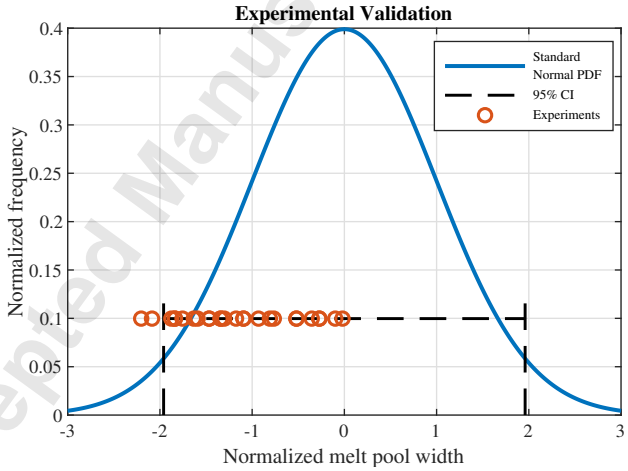

Figure 11. Experimental validation of the FEM model via UP.

design points to accelerate computations, in contrast to traditional equally spaced designs such as Latin Hypercube designs. We have demonstrated that the proposed framework is able to estimate the moments of the distribution of the model output using 70 simulations, yielding similar results to those obtained using brute force MC with 15,000 simulations. Finally, a very useful by-product of the UP framework is that the gPCE model can be regarded as a computationally efficient surrogate that can be used in lieu of the original computationally intensive physics-based model to generate sufficiently large numbers of simulations needed to conduct process planning and uncertainty analysis. Experimental validation of the two models was conducted whereby physical measurements of single-track melt pool widths were compared with the results from the UP

Accepted Manuscript Not Copyedited

Downloaded From: http://biomechanical.asmedigitalcollection.asme.org/ on 09/04/2018 Terms of Use: http://www.asme.org/about-asme/terms-of-use

Journal of Manufacturing Science and Engineering. Received November 08, 2017;
Accepted manuscript posted August 17, 2018. doi:10.1115/1.4041179
Copyright (c) 2018 by ASME

framework using a statistical hypothesis test.

Future research directions include applying this UP-based validation to multi-output computational models and conducting UP analysis through coupled (or hierarchical) physics-based models where the outputs of one model represent inputs to another subsequent model throughout the AM process chain (such as prediction of microstructure [58]). Uncertainty analysis through coupled physics-based models is an important topic that is crucial towards accelerating qualification and certification of AM-fabricated parts.

Acknowledgements

This work was supported by an Early Stage Innovations grant from NASA's Space Technology Research Grants Program, grant number NNX15AD71G. Portions of this research were conducted with High Performance Research Computing resources provided by Texas A&M University (http://hprc.tamu.edu/).

Nomenclature

AM Additive Manufacturing
L-PBF Laser-based Powder Bed Fusion
UQ Uncertainty Quantification
UP Uncertainty Propagation
ET Eagar-Tsai model
FETM Finite element thermal model
QoI Quantities of interest
gPCE Generalized polynomial chaos expansions
SA Sensitivity Analysis
MAE Mean absolute error
MC Monte Carlo

References

[1] Gustavo Tapia and Alaa Elwany. A review on process monitoring and control in metal-based additive manufacturing. *Journal of Manufacturing Science and Engineering*, 136(6):060801, 2014.

[2] Rajit Ranjan, Rutuja Samant, and Sam Anand. Integration of design for manufacturing methods with topology optimization in additive manufacturing. *Journal of Manufacturing Science and Engineering*, 139(6):061007, 2017.

[3] Marco Grasso, Vittorio Laguzza, Quirico Semeraro, and Bianca Maria Colosimo. In-process monitoring of selective laser melting: spatial detection of defects via image data analysis. *Journal of Manufacturing Science and Engineering*, 139(5):051001, 2017.

[4] Saad A Khairallah, Andrew T Anderson, Alexander Rubenchik, and Wayne E King. Laser powder-bed fusion additive manufacturing: Physics of complex melt flow and formation mechanisms of pores, spatter, and denudation zones. *Acta Materialia*, 108:36–45, 2016.

[5] W King, AT Anderson, RM Ferencz, NE Hodge, C Kamath, and SA Khairallah. Overview of modelling and simulation of metal powder bed fusion process at lawrence livermore national laboratory. *Materials Science and Technology*, 31 (8):957–968, 2015.

[6] Mahesh Mani, Shaw Feng, Brandon Lane, Alkan Donmez, Shawn Moylan, and Ronnie Fesperman. *Measurement science needs for real-time control of additive manufacturing powder bed fusion processes*. US Department of Commerce, National Institute of Standards and Technology, 2015.

[7] Donghua Dai and Dongdong Gu. Thermal behavior and densification mechanism during selective laser melting of copper matrix composites: simulation and experiments. *Materials & Design*, 55:482–491, 2014.

[8] Olaf Rehme. *Cellular design for laser freeform fabrication*. Cuvillier Göttingen, 2010.

[9] Johannes Trapp, Alexander M Rubenchik, Gabe Guss, and Manyalibo J Matthews. In situ absorptivity measurements of metallic powders during laser powder-bed fusion additive manufacturing. *Applied Materials Today*, 9:341–349, 2017.

[10] National Institute of Standards and Technology. Measurement science roadmap for metal-based additive manufacturing. Technical report, NIST, 2013. [Online]. Available from `https://www.nist.gov/sites/default/files/documents/el/isd/NISTAdd_Mfg_Report_FINAL-2.pdf`.

[11] Matthias Markl and Carolin Körner. Multiscale modeling of powder bed–based additive manufacturing. *Annual Review of Materials Research*, 46:93–123, 2016.

[12] M Matsumoto, M Shiomi, K Osakada, and F Abe. Finite element analysis of single layer forming on metallic powder bed in rapid prototyping by selective laser processing. *International Journal of Machine Tools and Manufacture*, 42 (1):61–67, 2002.

Accepted Manuscript Not Copyedited

Downloaded From: http://biomechanical.asmedigitalcollection.asme.org/ on 09/04/2018 Terms of Use: http://www.asme.org/about-asme/terms-of-use

Journal of Manufacturing Science and Engineering. Received November 08, 2017;
Accepted manuscript posted August 17, 2018. doi:10.1115/1.4041179
Copyright (c) 2018 by ASME

[13] Chinnapat Panwisawas, Chunlei Qiu, Magnus J Anderson, Yogesh Sovani, Richard P Turner, Moataz M Attallah, Jeffery W Brooks, and Hector C Basoalto. Mesoscale modelling of selective laser melting: Thermal fluid dynamics and microstructural evolution. *Computational Materials Science*, 126:479–490, 2017.

[14] Gustavo Tapia, Saad Khairallah, Manyalibo Matthews, Wayne E King, and Alaa Elwany. Gaussian process-based surrogate modeling framework for process planning in laser powder-bed fusion additive manufacturing of 316l stainless steel. *The International Journal of Advanced Manufacturing Technology*, pages 1–13, 2017.

[15] Qian Ye and Shikui Chen. Numerical modeling of metal-based additive manufacturing using level set methods. *Journal of Manufacturing Science and Engineering*, 139(7):071019, 2017.

[16] National Research Council et al. *Assessing the reliability of complex models: mathematical and statistical foundations of verification, validation, and uncertainty quantification*. National Academies Press, 2012.

[17] Ralph C Smith. *Uncertainty quantification: theory, implementation, and applications*, volume 12. Siam, 2013.

[18] Anthony O'Hagan. Polynomial chaos: A tutorial and critique from a statistician's perspective. *SIAM/ASA J. Uncertainty Quantification*, 20:1–20, 2013.

[19] TW Eagar and NS Tsai. Temperature fields produced by traveling distributed heat sources. *Welding journal*, 62(12): 346–355, 1983.

[20] Chandrika Kamath. Data mining and statistical inference in selective laser melting. *The International Journal of Advanced Manufacturing Technology*, 86(5-8):1659–1677, 2016.

[21] WE King, AT Anderson, RM Ferencz, NE Hodge, C Kamath, SA Khairallah, and AM Rubenchik. Laser powder bed fusion additive manufacturing of metals; physics, computational, and materials challenges. *Applied Physics Reviews*, 2(4):041304, 2015.

[22] Chandrika Kamath, Bassem El-dasher, Gilbert F Gallegos, Wayne E King, and Aaron Sisto. Density of additively-manufactured, 316l ss parts using laser powder-bed fusion at powers up to 400 w. *The International Journal of Advanced Manufacturing Technology*, 74(1-4):65–78, 2014.

[23] Edison A Bonifaz. Finite element analysis of heat flow in single-pass arc welds. *WELDING JOURNAL-NEW YORK-*, 79(5):121–s, 2000.

[24] JC Ion. Laser transformation hardening. *Surface Engineering*, 18(1):14–31, 2002.

[25] Maarten Van Elsen, Martine Baelmans, Peter Mercelis, and J-P Kruth. Solutions for modelling moving heat sources in a semi-infinite medium and applications to laser material processing. *International Journal of heat and mass transfer*, 50(23):4872–4882, 2007.

[26] Kubra Karayagiz, Alaa Elwany, Gustavo Tapia, Brian Franco, Luke Johnson, Ji Ma, Ibrahim Karaman, and Raymundo Arroyave. Numerical and experimental analysis of heat distribution in the laser powder bed fusion of ti-6 al-4 v. *IISE Transactions*, (just-accepted):1–44, 2018.

[27] Panagiotis Michaleris. Modeling metal deposition in heat transfer analyses of additive manufacturing processes. *Finite Elements in Analysis and Design*, 86:51–60, 2014.

[28] J Schilp, C Seidel, H Krauss, and J Weirather. Investigations on temperature fields during laser beam melting by means of process monitoring and multiscale process modelling. *Advances in Mechanical Engineering*, 6:217584, 2014.

[29] Deepankar Pal, Nachiket Patil, Kai Zeng, and Brent Stucker. An integrated approach to additive manufacturing simulations using physics based, coupled multiscale process modeling. *Journal of Manufacturing Science and Engineering*, 136(6):061022, 2014.

[30] Ali Foroozmehr, Mohsen Badrossamay, Ehsan Foroozmehr, and Sa'id Golabi. Finite element simulation of selective laser melting process considering optical penetration depth of laser in powder bed. *Materials & Design*, 89:255–263, 2016.

[31] David L Bourell, Ming C Leu, and David W Rosen. Roadmap for additive manufacturing: identifying the future of freeform processing. *The University of Texas at Austin, Austin, TX*, 2009.

[32] William E Frazier. Direct digital manufacturing of metallic components: vision and roadmap. *Direct Digital Manufacturing of Metallic Components: Affordable, Durable, and Structurally Efficient Airframes, at Solomons Island, MD*, 2010.

[33] Serguei Kolossov, Eric Boillat, Rémy Glardon, P Fischer, and M Locher. 3d fe simulation for temperature evolution in the selective laser sintering process. *International Journal of Machine Tools and Manufacture*, 44(2):117–123, 2004.

[34] Ibiye Aseibichin Roberts, CJ Wang, R Esterlein, M Stanford, and DJ Mynors. A three-dimensional finite element analysis of the temperature field during laser melting of metal powders in additive layer manufacturing. *International Journal of Machine Tools and Manufacture*, 49(12):916–923, 2009.

[35] F-J Gürtler, M Karg, K-H Leitz, and M Schmidt. Simulation of laser beam melting of steel powders using the three-dimensional volume of fluid method. *Physics Procedia*, 41:881–886, 2013.

[36] G Tapia, AH Elwany, and H Sang. Prediction of porosity in metal-based additive manufacturing using spatial gaussian process models. *Additive Manufacturing*, 12:282–290, 2016.

[37] Amir M Aboutaleb, Linkan Bian, Alaa Elwany, Nima Shamsaei, Scott M Thompson, and Gustavo Tapia. Accelerated process optimization for laser-based additive manufacturing by leveraging similar prior studies. *IISE Transactions*, 49

Accepted Manuscript Not Copyedited

Downloaded From: http://biomechanical.asmedigitalcollection.asme.org/ on 09/04/2018 Terms of Use: http://www.asme.org/about-asme/terms-of-use

Journal of Manufacturing Science and Engineering. Received November 08, 2017;
Accepted manuscript posted August 17, 2018. doi:10.1115/1.4041179
Copyright (c) 2018 by ASME

(1):31–44, 2017.

[38] Marc C Kennedy and Anthony O'Hagan. Bayesian calibration of computer models. *Journal of the Royal Statistical Society. Series B, Statistical Methodology*, pages 425–464, 2001.

[39] Norbert Wiener. The homogeneous chaos. *American Journal of Mathematics*, 60(4):897–936, 1938.

[40] Habib N Najm. Uncertainty quantification and polynomial chaos techniques in computational fluid dynamics. *Annual review of fluid mechanics*, 41:35–52, 2009.

[41] OM Knio and OP Le Maitre. Uncertainty propagation in cfd using polynomial chaos decomposition. *Fluid Dynamics Research*, 38(9):616–640, 2006.

[42] Serhat Hosder, Robert W Walters, and Rafael Perez. A non-intrusive polynomial chaos method for uncertainty propagation in cfd simulations. *AIAA paper*, 891:2006, 2006.

[43] Géraud Blatman and Bruno Sudret. An adaptive algorithm to build up sparse polynomial chaos expansions for stochastic finite element analysis. *Probabilistic Engineering Mechanics*, 25(2):183–197, 2010.

[44] Avinash Prabhakar, James Fisher, and Raktim Bhattacharya. Polynomial chaos-based analysis of probabilistic uncertainty in hypersonic flight dynamics. *Journal of guidance, control, and dynamics*, 33(1):222, 2010.

[45] Recep M Gorguluarslan, Seung-Kyum Choi, and Christopher J Saldana. Uncertainty quantification and validation of 3d lattice scaffolds for computer-aided biomedical applications. *Journal of the Mechanical Behavior of Biomedical Materials*, 71:428–440, 2017.

[46] Dongbin Xiu and George Em Karniadakis. The wiener–askey polynomial chaos for stochastic differential equations. *SIAM journal on scientific computing*, 24(2):619–644, 2002.

[47] Giovanni Sansone. *Orthogonal functions*, volume 9. Courier Corporation, 1959.

[48] Hui Zou and Trevor Hastie. Regularization and variable selection via the elastic net. *Journal of the Royal Statistical Society: Series B (Statistical Methodology)*, 67(2):301–320, 2005.

[49] Jerome Friedman, Trevor Hastie, and Rob Tibshirani. Regularization paths for generalized linear models via coordinate descent. *Journal of statistical software*, 33(1):1, 2010.

[50] Chih-Wei Hsu, Chih-Chung Chang, Chih-Jen Lin, et al. A practical guide to support vector classification. 2003.

[51] Art B Owen. Variance components and generalized sobol'indices. *SIAM/ASA Journal on Uncertainty Quantification*, 1(1):19–41, 2013.

[52] Bruno Sudret. Global sensitivity analysis using polynomial chaos expansions. *Reliability Engineering & System Safety*, 93(7):964–979, 2008.

[53] Aerospace Specification Metals Inc. AISI type 430 stainless steel annealed sheet, Aug 2017. URL `http://asm.matweb.com/search/SpecificMaterial.asp?bassnum=mq430an`.

[54] Paul Bratley and Bennett L Fox. Algorithm 659: Implementing sobol's quasirandom sequence generator. *ACM Transactions on Mathematical Software (TOMS)*, 14(1):88–100, 1988.

[55] Wei Chen, Lusine Baghdasaryan, Thaweepat Buranathiti, and Jian Cao. Model validation via uncertainty propagation and data transformations. *AIAA journal*, 42(7), 2004.

[56] Richard G Hills and Timothy G Trucano. Statistical validation of engineering and scientific models: Background. *Sandia National Laboratories, Albuquerque, NM, Report No. SAND99-1256*, 1999.

[57] George EP Box and David R Cox. An analysis of transformations. *Journal of the Royal Statistical Society. Series B (Methodological)*, pages 211–252, 1964.

[58] Jeff Irwin, Edward W Reutzel, Pan Michaleris, Jay Keist, and Abdalla R Nassar. Predicting microstructure from thermal history during additive manufacturing for ti-6al-4v. *Journal of Manufacturing Science and Engineering*, 138 (11):111007, 2016.

Accepted Manuscript Not Copyedited

Downloaded From: http://biomechanical.asmedigitalcollection.asme.org/ on 09/04/2018 Terms of Use: http://www.asme.org/about-asme/terms-of-use

Journal of Manufacturing Science and Engineering. Received November 08, 2017;
Accepted manuscript posted August 17, 2018. doi:10.1115/1.4041179
Copyright (c) 2018 by ASME

List of Figures

1 Computational complexity of the gPCE model based on values for t and q. 6
2 Example of the thermal field solution after simulation of the ET model, with a black contour line added at melting temperature. Plane xy shown at level $z = 0$, and plane xz shown at level $y = 0$. 10
3 Sparse gPCE with adaptive sampling flow chart. 11
4 Performance of the sparse gPCE adaptive sampling algorithm. **a)** CV error history after 7 iterations showing convergence. **b)** Performance of the gPCE model over a test set. 12
5 gPCE-based global sensitivity analysis. **a)** Normalized single effect and two-way interaction indices. **b)** Normalized Total Sensitivity indices. 13
6 Histogram with a kernel density estimate (red line) after 15,000 ET simulations from MC random sampling. 14
7 Experimental measurements of single tracks on a 430F Stainless Steel bare plate. **a)** Optical microscopy image. **b)** Dataset distribution. 15
8 Experimental validation of the ET model via UP. 16
9 Application of the sparse and adaptive gPCE framework to the FEM model. **a)** CV error path after 8 iterations. **b)** gPCE-based sensitivity analysis showing normalized single effect and two-way interactions Sobol indices. 17
10 Experimental measurements of Ti-6Al-4V single tracks. **a)** Optical microscopy image. **b)** Dataset distribution. 18
11 Experimental validation of the FEM model via UP. 18

List of Tables

1 Melt pool width statistical distribution moments. 14
2 Melt pool width statistical moments based on FEM model and gPCE. 16

Accepted Manuscript Not Copyedited

Downloaded From: http://biomechanical.asmedigitalcollection.asme.org/ on 09/04/2018 Terms of Use: http://www.asme.org/about-asme/terms-of-use